Journal of Geographical Systems (2005) 7: 273–290
DOI 10.1007/s10109-005-0007-4

ORIGINAL ARTICLE

Nicholas J. Tate · Chris Brunsdon
Martin Charlton · A. Stewart Fotheringham
Claire H. Jarvis

Smoothing/filtering LiDAR digital surface models. Experiments with loess regression and discrete wavelets

Published online: 6 October 2005

Abstract This paper reports on the smoothing/filtering analysis of a digital surface model (DSM) derived from LiDAR altimetry for part of the River Coquet, Northumberland, UK using loess regression and the 2D discrete wavelet transform (DWT) implemented in the S-PLUS and R statistical packages. The chosen method of analysis employs a simple method to generate noise' which is then added to a smooth sample of LiDAR data; loess regression and wavelet methods are then used to smooth/filter this data and compare with the original smooth' sample in terms of RMSE. Various combinations of functions and parameters were chosen for both methods. Although wavelet analysis was effective in filtering the noise from the data, loess regression employing a quadratic parametric function produced the lowest RMSE and was the most effective.

N. J. Tate (✉) · C. H. Jarvis
Department of Geography, University of Leicester,
Leicester, LE17RH, UK
E-mail: n.tate@le.ac.uk
Tel.: +44-116-2231320
Fax: +44-116-2523854

C. Brunsdon
School of Computing, University of Glamorgan,
Pontypridd, Wales, CF37 1DL, UK

M. Charlton · A. S. Fotheringham
National Centre for Geocomputation,
National University of Ireland, Maynooth,
County Kildare, Ireland

Keywords Digital surface model · LiDAR data

1 Introduction

The paper is concerned with the smoothing/filtering of a LiDAR- (*Li*ght *D*etection *a*nd *R*anging)[1]—derived digital surface model (DSM), using loess regression and wavelet functions. The report focuses specifically on a pilot analysis of a 2-m resolution gridded DSM derived from LiDAR for part of the River Coquet, Northumberland, UK. LiDAR is an *active* technique of remote sensing (Lillesand et al. 2004) typically involving an airborne sensor that emits and collects laser light reflected off the Earth's surface to construct a DSM (Huising and Gomes-Pereira 1998; Wehr and Lohr 1999; Dubayah et al. 2000). Interaction of the laser light with the Earth's surface is a potential source of both systematic and random errors (Huising and Gomes-Periera 1998) and as a result DSMs will require error removal during post-processing. Wehr and Lohr (1999) have emphasised the importance of post-processing to the quality of the final DSM, and have noted that because of this many methods have been developed on a proprietary basis only. The use of LiDAR as a data source for the construction of DSMs and DEMs is becoming increasingly commonplace. It is therefore timely that methods to smooth/filter LiDAR data are explored.

Essentially, the motivation behind this study is to develop methods to recover a surface of unknown smoothness from a noisy LiDAR DSM. In places where the DSM is already reasonably free of noise, one does not want to apply very much smoothing/filtering—since although filtering leads to noise reduction, over-filtering will distort the shape of the underlying surface to some extent. The aim is thus to get the oil to the squeak' in the sense of applying noise smoothers/filters only in localities where noise exists. Although the focus of this paper is on the use of loess regression and wavelets, many other approaches exist for the identification and removal of both systematic and random errors in DEMs and DSMs. Systematic errors can be removed by some form of low-pass filtering and subsequent adjustment of elevation values (e.g., Albani and Klinkenberg 2003). Other error removal methods include the outlier detection methods described in Lòpez (2002), and 2D Kalman filtering (Wang 1998).

Loess regression and wavelets are both *local* statistical methods that are particularly appropriate for the analysis of *non-stationary* spatial data series that are often encountered in physical geography, of which a set of sampled elevations in the form of a DSM or Digital Elevation Model (DEM) is an example. Both methods have been widely used in mathematics and image processing, but in contrast they have been little employed in geography and GIS. In this paper, we explore the application of these methods for the removal of error in the form of noise' introduced to a portion of a LiDAR-derived DSM.

[1] known also as a *laser altimeter* (Dubayah et al. 2000)

This paper is organised into five sections. Section 2 covers the mathematics of loess regression and wavelet transforms and considers the appropriateness of both methods for the analysis of geographic data series. In Sect. 3, we outline the characteristics of the study area and the LiDAR data set, the error model and analyses are reported in Sect. 4 and finally the software used for the experiments. The results from both methods are described and discussed in Sect. 4 with concluding comments in Sect. 5.

2 Loess regression and wavelet analysis

Spatial *non-stationarity* (usually in the form of trends in the mean and variance) provides a particular challenge for the application of traditional statistical methods borrowed from the time series analysis domain, such as those based on autocorrelation and Fourier methods (e.g. power spectral density) that are employed in the analysis of geospatial data. Fourier methods in particular are often described as possessing good *frequency localisation* but poor *temporal localisation* characteristics (e.g., Kumar and Foufoula-Georgiou 1997). This limitation has been related to the well-known result of the Heisenberg Uncertainty Principle (Hubbard 1996: 50) that dictates that one cannot measure with arbitrarily high resolution in both time *and* frequency' (Kumar and Foufoula-Georgiou 1997: 387, emphasis added). In a geographical context, this translates to poor *spatial localisation*. In other words, the ability to resolve frequencies in a data series is achieved at the expense of averaging, resulting in poor resolution in the spatial domain. Such averaging by definition requires that the data are consistent with a stationary model. This partly explains why methods that require either weaker models of stationarity (such as the intrinsic stationarity of variogram analysis: see Myers 1989) or no models of stationarity at all are often more attractive for geographical data analysis (see Atkinson 2001). Loess regression and wavelet analysis are both *local* methods of analysis that have been applied to the smoothing and filtering of data series, and as such they are suited to much geospatial data that are consistent with a non-stationary mathematical model.

2.1 Loess regression

Loess regression is a form of local regression model (Cleveland et al. 1992; Cleveland and Loader 1996). Although recently popularised in the late 1970s by Cleveland and co-workers, local regression has various historical roots that can be traced back to nineteenth Century Europe (Cleveland and Loader 1996). In local regression a function of unknown algebraic form in the model $y = f(x) + e$ is estimated given a set of data pairs (x_i, y_i) for $i = 1,...,n$. The approach used is to fit a parametric curve, such as a straight line or a quadratic, in the locality of a given x value, weighting each of the (x_i, y_i) pairs according to the nearness of x_i to x. Approximating a function locally in this way is known as *parametric localisation* (Cleveland and Loader 1996).

Basic local regression requires decisions to be made regarding the weights, the bandwidth around each x, the parametric functions to be fitted and the criterion of fitting (Cleveland and Loader 1996). The ingredients of the loess regression adopted in this study are a particular weight function, termed the *tricube* weight function, along with bandwidths for each x chosen on the basis of the nearest fixed percentage of the rest of the data set (this percentage is termed the *span*), local polynomial parametric functions, and an iterative down-weighting fitting criterion (Cleveland and Loader 1996). For a given x and bandwidth h, the tricubic weight applied to each of the n (x_i, y_i) is:

$$w_i(x) = \max\left\{0, \left(1 - \left(\frac{|x - x_i|}{h}\right)^3\right)^3\right\}$$

Thus, for any given x an associated set of n weights is generated. These are used to calibrate parameter estimates for the local parametric curve. This gives a unique set of parameters centred on x, which may be used to estimate $f(x)$. The choice of bandwidth h determines the smoothness of the estimate of $f(x)$. In loess regression, h takes different values for each x as described above. Thus, each h is chosen so that a given proportion (the span) of all of the data is non-zero weighted. As x changes, the parameter estimates change with x so that the estimate $f(x)$ varies continuously. A final feature of loess regression is that there is some robustness to outliers. This is achieved using an iterative, multi-pass approach. A basic loess regression is fitted as set out above, and for each x_i a value of $f(x_i)$ is estimated. The residuals $x_i - f(x_i)$ are then computed. A very large absolute value of residual for a given i suggests that observation i is an outlier. Such observations are down-weighted (or if the outlier is very large, zero-weighted) and the loess procedure is run again to give a more robust estimate of $f(x)$. The re-weighting procedure is typically to multiply the existing weights, w_i, by a factor K_i, where

$$K_i = \min\left\{1, \max\left\{0, \left(1 - \frac{e_i}{s_e}\right)^2\right\}\right\}$$

and e_i is the residual for observation i and s_e is the standard deviation of the residuals. Any residual less than 2SD results in no change in weighting, and any over three standard deviations results in zero weighting. Residuals between two and three standard deviations are progressively down-weighted on a linear scale. Typically, as in this study, loess regressions have two or three passes of the above procedure.

2.2 Wavelet analysis

Wavelet analysis has been developed and popularised over the last 20 years in a wide number of scientific contexts. In a GIS context applications have ranged from the scale-based filtering and construction of multi-resolution terrain models (Gallant and Hutchinson 1997; McArthur et al. 2000; Bjørke

and Nilsen 2003), point pattern analysis (Rosenberg 2004) to more general spatial data analysis (Morehart et al. 1999; Csillag and Kabos 2002). The detailed mathematics are beyond the scope of this paper, and can be found in Daubechies (1992), Bruce and Gao (1995), Lark and Webster (1999) and a useful paper by Abramovich et al. (2000). It should be noted form the outset that practical implementation of the DWT within computer software such as S-PLUS often makes use of fast algorithms, for example the O(n) complexity algorithm developed by Mallat (1989) employing a hierarchical series of low and high pass filters (Abramovich et al. 2000)—one of a class of Fast Wavelet Transforms (Strang 1994). The basic treatment here will be based primarily on the 1D DWT of $z(x)$ although this can be easily extended to the 2D DWT of $z(x,y)$. Essentially the method involves the approximation of a function of interest $z(x)$ by the series expansion of orthonormal / (*scaling* wavelet) and w (*mother* wavelet) basis functions and wavelet transform coefficients d and s. Adopting the notation of Bruce and Gao (1995) $w_{j,k}(x)$ and $/_{j,k}(x)$ are obtained by a process of dilating the wavelet functions to M levels (or scales) and translating by k along the function of interest where (Bruce and Gao 1995; Abramovich et al. 2000; Jiang et al. 2000; Csillag and Kabos 2002):

$$w_{j;k}(x) = 2^{-j/2} w\left(2^{-j}x - k\right); \quad /_{j;k}(x) = 2^{-j/2} /\left(2^{-j}x - k\right); \quad j = 1; 2; \ldots; M$$

for $j \in \mathbf{Z}$ and $k \in \mathbf{Z}$ where $\mathbf{Z}$ is the set of integers.

As noted by Daubechies (in Hubbard 1996: 49–50) the ability to resize/dilate wavelets means that both big wavelets—localised in *frequency*—and small wavelets—localised in *time*—can be used, giving wavelets good temporal *and* frequency localisation. Wavelet functions are only required to be a waveform with a compact support in temporal and frequency domains with zero mean (i.e. $\int_{-1}^{1} w(x)\,dx = 0$) and unit square norm (i.e. $\int_{-1}^{1} w(x)^2\,dx = 1$) for mother wavelets, and unit mean and unit square norm for scaling wavelets (Kumar and Foufoula-Georgiou 1997; Lark and Webster 1999). Consequently, there are a large number of wavelet functions available, which only differ in detail. Examples of two wavelets are displayed in Fig. 1: specifically the simple Haar wavelet and the more complex Daubechies length eight wavelet of order 4. Note that the definition of order here varies according to the kind of wavelet, but typically wavelets of higher order tend to be more complex in shape. For the Daubechies wavelets, order 4 implies four vanishing moments i.e. that the first four moments of the wavelet generating function are zero.

The wavelet transform coefficients d and s—which from Bruce and Gao (1995) correspond to the high frequency detail' and low frequency smooth' components of the function respectively and are approximated as follows (Bruce and Gao 1995; Csillag and Kabos 2002):

$$d_{j;k} \approx \int z(x)\, w_{j;k}(x)\, dx; \quad s_{M;k} \approx \int z(x)\, /_{M;k}(x)\, dx; \quad j = 1; 2; \ldots; M$$

The description so far has been in the context of 1D transform. The DWT in 2D is a simple extension of the DWT in 1D (Lark and Webster 2004 which

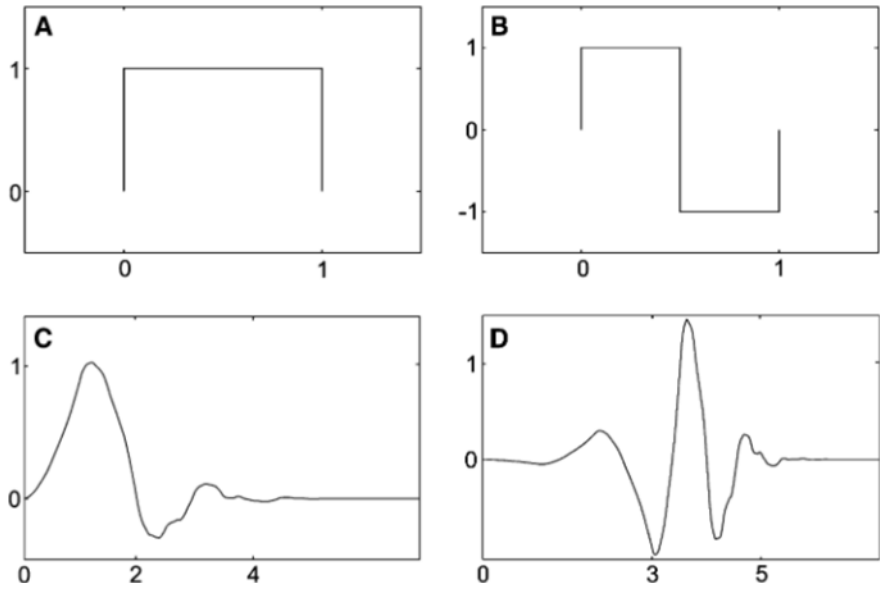

Fig. 1 Scaling / and mother w wavelet functions for Haar (**A** and **B**, respectively) and Daubechies length 8 order 4 (**C** and **D**, respectively) wavelets

should be consulted for further details). Essentially this proceeds by the application of the 1D DWT on the *columns* of data corresponding to the 2D input image/array, the storage of the resulting wavelet transform coefficients in an intermediate 2D matrix, and the application of the 1D DWT on the *rows* of this matrix (Lark and Webster 2004). For each level M, four sets of coefficients are produced:one set of smooth (scaling) coefficients **S**, and three sets of detail (wavelet) coefficients: *vertical* $\mathbf{D_V}$ (row smooth, column detail coefficients), *diagonal* $\mathbf{D_D}$ (row detail, column detail coefficients) and *horizontal* $\mathbf{D_H}$ (row detail, column smooth coefficients). These are typically stored as sub-matrices of a larger 2 by 2 matrix (Lark and Webster 2004), specifically:

$$\begin{bmatrix} \mathbf{S} & \mathbf{D_H} \\ \mathbf{D_V} & \mathbf{D_D} \end{bmatrix}$$

Different wavelet software stores these coefficients in slightly different locations (Davis and Nosratinia 1999; Bjørke and Nilsen 2003) and within S-PLUS, this arrangement is:

$$\begin{bmatrix} \mathbf{D_H} & \mathbf{D_D} \\ \mathbf{S} & \mathbf{D_V} \end{bmatrix}$$

An image of Professor Michael Goodchild (Geography, UCSB) and the results from using the S-PLUS 2D DWT of this image for three levels ($M = 3$) of wavelet transformation are displayed in Fig. 2. The correspon-

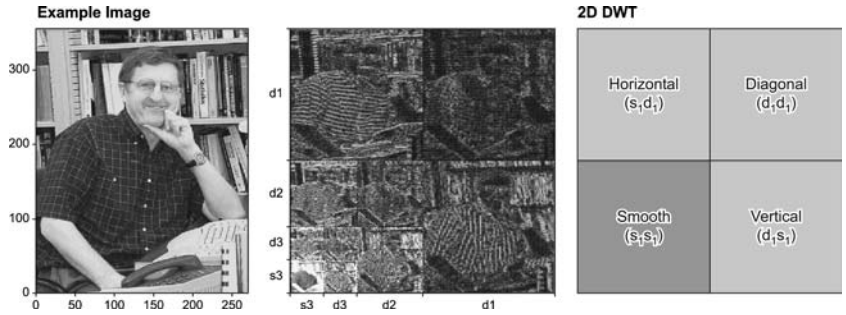

Fig. 2 Example image with the results of a three level 2D DWT. The combination of detail and smooth coefficients are mapped for level 1

dence of the detail coefficients at level 1 to the vertical, diagonal and horizontal elements of the image (note the lines on the shirt) can been seen clearly from this figure.

A utility of the DWT is that the original function [$z(x)$ or $z(x,y)$] can be perfectly recovered by inversely transforming the scaled/translated wavelet function pair / and w and wavelet transform coefficients d and s. This, and the fact that a considerable number of the detail coefficients d are zero, makes the method very attractive for both the scale-based generalisation and the efficient storage of functions (Graps 1995). It is for example the basis for the JPEG2000 compression technique (Taubman and Marcellin 2001). Wavelet analysis is also attractive from the perspective of a form of data filtering known as *signal denoising*. This can be accomplished by reducing, or setting to zero, a portion of the detail' coefficients d and then reconstructing the original function $z(x)$ (Graps 1995). Donoho and Johnstone's (1994, 1995) wavelet shrinkage methods have been widely adopted in signal and image processing, and are based on non-linear soft-thresholding of the transform coefficients (Taswell 2000). The aim of wavelet shrinkage is to apply a low pass filter such that noisy spatial data are impacted upon but areas where there is little noise remain untouched, fitting well with the de-noising' goal of this paper.

Our work adopts the *sureshrink* procedure of Donoho and Johnstone (1995), which achieves wavelet shrinkage using the following method, as set out by its authors:

1. Apply wavelet transform to the noisy surface: this provides a set of wavelet detail coefficients (which at this stage are also noisy)—if the surface grid heights from LiDAR are $\{y_i\}$, call these coefficients $\{d_{j,k}\}$, where the indices denote the kth wavelet coefficient at level j. Higher levels of j denote higher frequency wavelets.
2. Threshold the noisy wavelet coefficients: This is done by replacing each $\{d_{j,k}\}$, with sgn $(y_{j,k})$ $(|y_{j,k}|\text{-}t_j)_+$. Any coefficients whose absolute value is less than t_j is set to zero, and other coefficients are shrunk' towards zero by an amount t.

3. Choose thresholds t_k for each wavelet level using Stein's unbiased estimate of risk (SURE; Stein 1981).

Typically, for lower frequency levels of j, the values of t_k are very small, leaving the coefficients virtually untouched, but for high-frequency levels values of t_k are higher, so that a greater degree of shrinkage to zero occurs. In areas where there is little noise, the values of $d_{j,k}$ will be low for high frequency j, and the shrinkage to zero will have little effect on the overall wavelet profile. However, in noisy regions, the shrinkage of the higher frequency $d_{j,k}s$ will have a smoothing effect, as desired. This approach can be applied to several types of wavelet, for example the commonly used Haar or Daubechies wavelets.

Wavelet-based signal denoising has been employed frequently in the context of removing the speckle in SAR images (e.g., Fukuda and Hirosawa 1998; Argenti and Alparone 2002; Dai et al. 2004) yet only infrequently in the context of filtering terrain data (e.g., Wang and Trinder 2002; Zatelli and Antonello 2002). This may be due to the fact that DEMs are typically interpolation-based and require little denoising, whereas SAR and LiDAR DSMs are measurement-based and the measurement process introduces noise, and requires some degree of pre-processing to remove noise and estimate the underlying surfaces.

3 Methods

3.1 Study area and data preprocessing

A LiDAR DSM created by the UK Environment Agency for a 1-km square section of the River Coquet in Northumberland provided the data set for analysis (Fig. 3; Charlton et al. 2003). The Coquet rises on the Scottish border and flows east about 80 km to its mouth at Amble. The catchment of the river is around 650 km^2. The location of the 1 km square tile of interest is at Brinkburn, which lies about 16 km inland (Ordnance Survey tile NZ1198). The River Coquet in this tile flows first through an unstable reach with its bank stability related to the incidence of adjacent tree cover, and then enters an incised conveyance channel with bedrock outcrops (Newson 2005). It was felt that this topographic variety would provide a range of surfaces for the experiment. The DSM was formed by interpolating the original first return LiDAR data obtained from an airborne ALTM400 in a Cessna 404 flown in March 1998 onto a grid. This is a narrow band instrument that produces a semi-regular array of spot heights between 1 and 4 m. Although commonly both first return data (corresponding to vegetation/building surface), and last return data (penetrating elevation to some degree) are collected from LiDAR instruments, only the first return data are used here. The data were processed in June 1998 using the WGS84 datum, and then transformed to OSGB36. They were then interpolated onto a 2×2 m^2 regular grid by the Environment Agency. There are a maximum of 250,000 observations in the file for each tile, with each observation consisting of a triplet $\{x,y,z\}$. A hill-

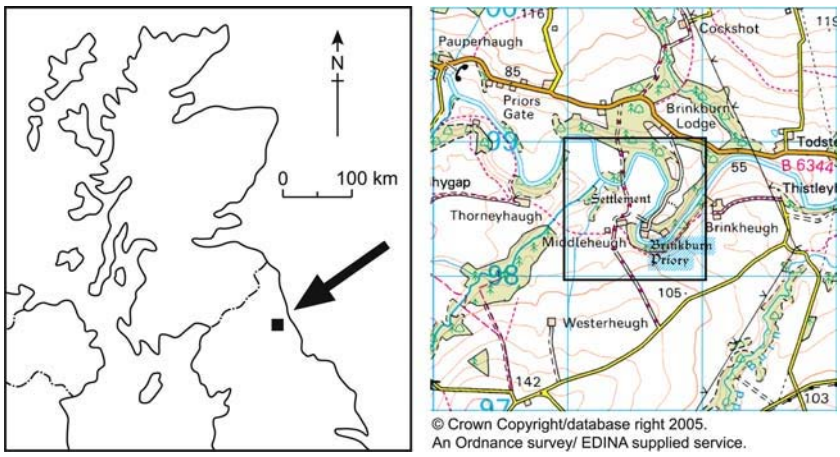

Fig. 3 Location map for the study area

shade of the raw 1 km square DSM can be seen in Fig. 4 (with an area of gross error in the SW omitted to improve the visualisation).

3.2 Error model

In order to evaluate the ability of both loess regression and wavelets to smooth/de-noise data, the approach was adopted of taking a known' surface, adding some noise to it, and then to smooth/filter the noise with each method. Since the task of the smoothing technique is to recover the known surface, then the success of this can be assessed by computing the root mean square error (RMSE) between the known surface, and that returned by the

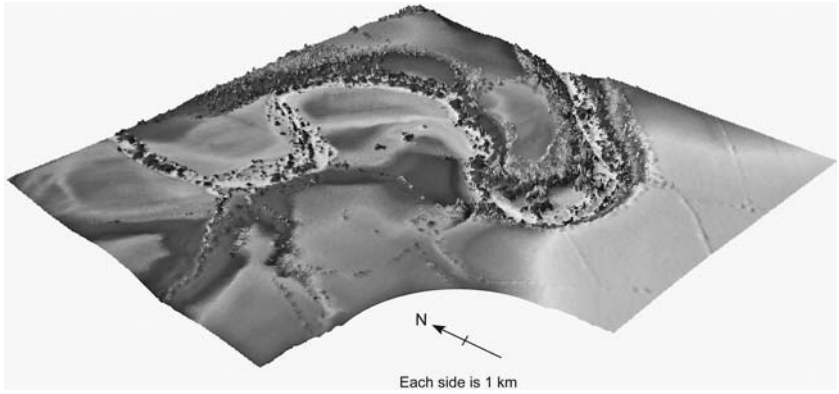

Fig. 4 Perspective view of the study area with the problematic zone in the SW removed

smoothing technique. It is on the basis of this validation technique, that the RMSE values quoted in this study are obtained. Two key issues here are the nature of the noise that is added to the known surface, and the choice of the known surface itself. The choice of surface was based on identifying a 120×120 m area of terrain that appeared to display little noise' in the LiDAR data (location S2 in Fig. 5). It was felt that this was a better option in contrast to using an artificially generated surface, say on the basis of some mathematical function $z=f(x,y)$. A simple reason for this approach is that the underlying surface used in the evaluation is geographically realistic and as such is one that is likely to occur in practice. It may therefore have characteristics that are not adequately encapsulated by some choice of function.

The choice of the noise model was more complex. It would be unrealistic to assume that the error in each LiDAR pixel would be uncorrelated to its neighbours, but at this stage it is difficult to ascertain the exact structure of the autocorrelation: LiDAR data are subject to a wide range of systematic errors which common to active systems are a combination of sensor and surface characteristics (Huising and Gomes-Pereira 1998; Wehr and Lohr 1999). Also, an inspection of the spikes' in the raw LiDAR surface model (these are apparent in Fig. 5—see later explanation) suggested that a

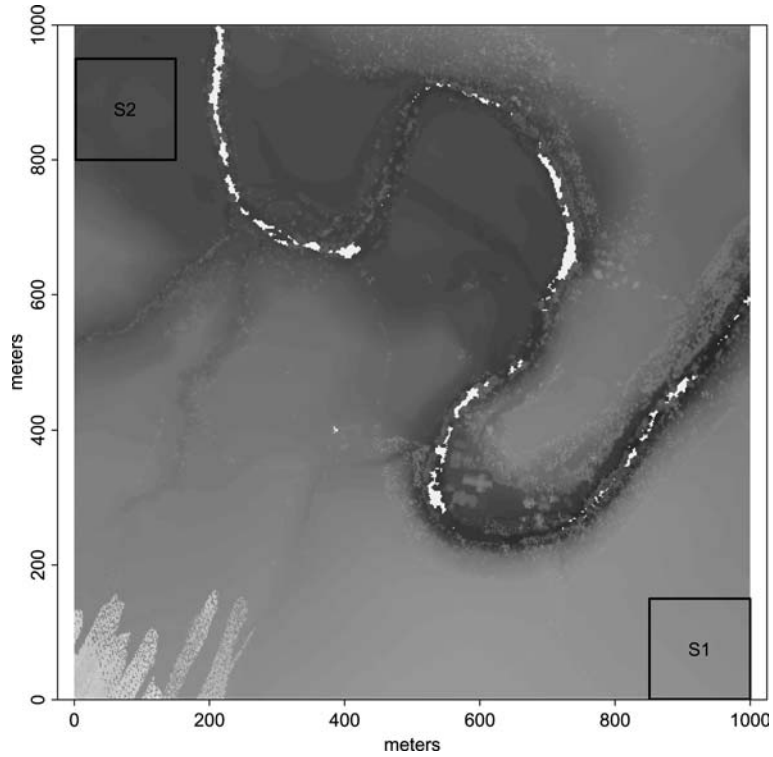

Fig. 5 Location of sample sites. S2 area of little noise'; S1 used to model error

Gaussian distribution is also unlikely. These combined factors make it difficult to justify the methodology of assuming an autocorrelated Gaussian error model, and simulating error terms based on this. Hence the following approach was adopted:

1. To select another section of the study area of exactly the same size as the known' surface, but that is considered to be more noisy (location S1 in Fig. 5).
2. To identify errors using a relatively crude method such as a global' simple planar regression (that is, fitting a model of the form $z = a + bx + cy$) to identify level of error on a pixel-by-pixel basis. Note that this approach is only appropriate in a study area where the landscape is close to a plane—as is the case for S1.
3. Add this grid of errors' to the known surface S2.

Thus, the errors found in step 2 are treated as the simulated noise in step 3. The errors generated from this approach should have the characteristics of real world' LiDAR errors—and therefore we have sidestepped the issue of choosing a model for noise by using some real world' noise. The modelled noise found in this algorithm is shown in Fig. 6. The Figures suggest that the noise may well be non-Gaussian and autocorrelated, although the degree of autocorrelation does not seem constant over the study area. There are also a number of high positive spikes. Since simple autocorrelated Gaussian errors do not exhibit these properties, it seems reasonable, at least at this initial stage, to adopt the approach outlined above. An additional reason for using the residuals from the relatively crude global plane-fitting method to obtain a model of noise is that this model is different to the loess regression and wavelet methods, and there it should minimise any bias in a comparative

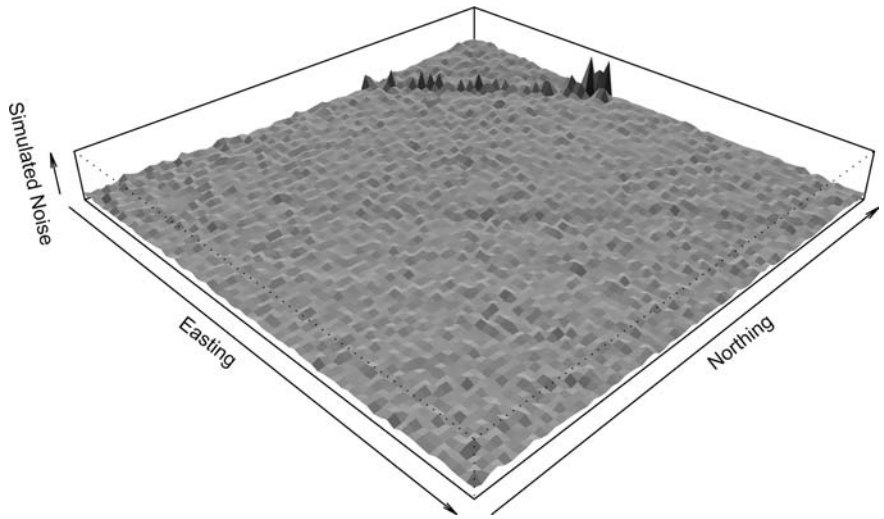

Fig. 6 Simulated errors based on residuals from a global regression applied in S1

assessment of the latter two methods. In many situations it would be difficult to justify this approach—however, the particular sample of location S1 is essentially a featureless plane. In this instance, extraction of the error term as residuals from the regression model is justifiable. The idea here is to borrow strength' from this particular location in order to simulate errors in other locations. Whereas we acknowledge that this approach does possess some shortcomings—particularly that a simple regression cannot recover error perfectly, and we are assuming that terrain complexity has no influence on the error—we feel that at least initially, being able to produce a set of errors close' to the real world outweighs the benefits of modelling random error terms in some more analytical way. It is proposed at a later date to compare this approach to one using simulated modelled errors.

3.3 Software

In order to generate a smooth/de-noised surface from S2, the R implementation of loess regression as described in Sect. 2.1 was applied using both linear and quadratic parametric functions of varying span. Note that since the LiDAR data are spaced on a regular grid, span and bandwidth are nearly equivalent in this study.

The 2D DWT-based wavelet smoothing analysis was implemented in both the S-PLUS and R statistical packages, the latter employing a version of Donoho and Johnstone's *sureshrink* algorithm (Whitcher 2004). A modification of wavelet shrinkage denoising was used in the context of the S-PLUS statistical software. This method involved writing an automated S-PLUS script which iterated the type of wavelet used, the percentage of detail coefficients (1–100%), and the number of levels or levels in the analysis (1–4), shrinking on the basis of coefficient magnitude. The S-PLUS WAVELETS library (S-PLUS 2000 version) allows up to 40 types of wavelet to be used, although with the geometric progression employed in the DWT and the finite grid size, the choice of certain wavelets limits the number of levels in the analysis without boundary correction. It should be noted in passing that source code for the DWT is available in Press et al. (1992).

4 Loess/wavelet results and discussion

4.1 Loess regression smoothing

The resulting RMSE (in metres) for both linear and quadratic functions of loess regression and varying span h are displayed in Fig. 7. From this analysis the minimum RMSE of 0.014 was obtained from a quadratic function with a span of around 0.01, which on the regular grid is equivalent to a bandwidth h of about 10 m. In contrast the minimum RMSE of 0.019 from the planar function was obtained from a span of 0.007 (about 7 m).

An interesting issue arises from this loess regression analysis: it seems that the local quadratic model outperforms the local planar model, but in addition to this it seems that the best span for a quadratic surface is higher than

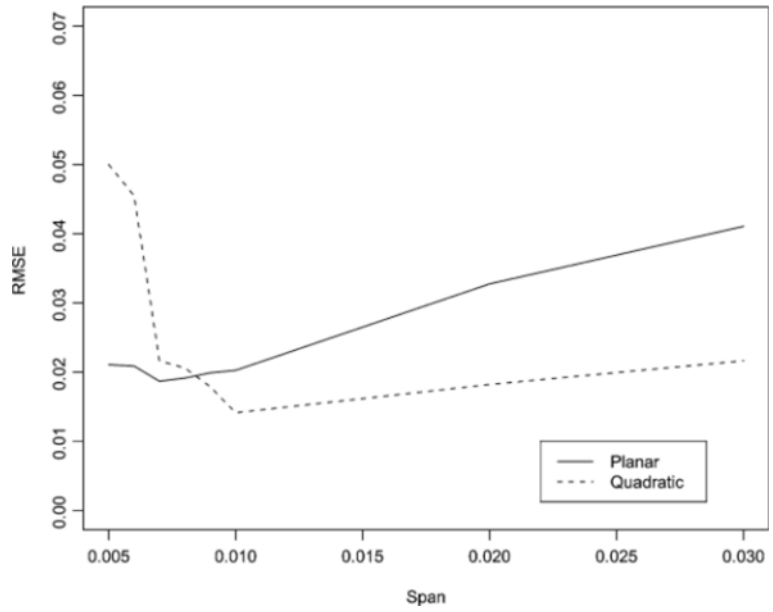

Fig. 7 Performance of Loess regression smoothing

that for a locally linear surface. This raises a question of scale—it seems that if one wishes to treat a terrain as locally planar, one must consider a smaller spatial window than if one is to treat a terrain as locally quadratic. This is perhaps not surprising—many terrain features are remarkably similar to quadratic forms reflecting naturally occurring features such as ridges, valleys, hills and lakes (or at least the land levels surrounding lakes) and this is reflected in the widespread use of quadratic polynomials to model various types of landforms (e.g., Schmidt et al. 2003; Wood 1998). The only way to approximate, say, a valley using planes is to subdivide it into smaller relatively flat sub-areas, and to find approximating planes for each of these. This in itself raises some interesting theoretical issues relating to scale—depending on how one is modelling a terrain, optimal' scales will differ. Similarly, multi-scale comparisons (such as visualising loess smoothes over a variety of spans) could also yield different results depending on the local model used.

However, as well as this extra dimension of complexity in the analysis of scales, some interesting potential applications arise from these findings, that may provide a link between terrain filtering and the quadratic-based landscape classification work of Wood (1996, 1998). From the latter, we know that by looking at the coefficients of local quadratic models, one can clearly determine whether the quadratic curve is a valley, a peak, a ridge or some other kind of quadratic form, and therefore assign a classification to the local land feature. For example, one could check whether the local quadratic surface has a maximum, and if it does, whether the maximum falls inside the regression window. If it does, this suggests that one is in the presence of a hilltop. In the context of terrain filtering, this information could be used as

part of a rule-based generalisation process, or a two pass smoothing/filtering method. For the first application, different surface generalisation algorithms could be applied to different kinds of terrain feature, with the output of the quadratic modelling used as input to set algorithm selection rules. For the second application, use could be made of filtering methods that are less likely to move extreme points (peaks, troughs) in those areas where these features are detected from the local quadratic surface fit.

4.2 Wavelet filtering

The filtered/denoised surface generated by each iteration of the automated wavelet programme was compared against the original noiseless surface and the RMSE calculated. Surfaces analysed to three levels with a default boundary condition generated the lowest RMSE estimates for the majority of wavelets. The RMSE results (in metres) for a three level calculation for 40 wavelets retaining varying percentages of coefficients are displayed in Fig. 8.

The results demonstrate that analysis with a biorthogonal v-spline wavelet vs2 (for definition see Bruce and Gao 1995: 294) produced the lowest RMSE estimate (0.0374) that was obtained whilst retaining 10% of the coefficients. Plan and perspective views of the original, noisy and filtered DSMs for this wavelet/coefficient choice can be seen in Fig. 9, to visualise the success of the wavelet smoothing procedure employed in this way.

Iterating the analysis through several wavelets using the *sureshrink* algorithm in the R software (a total of 17, listed in Table 1) and calculating the RMSE enabled a minimum RMSE of 0.033 to be obtained for the Fejer–Korovkin wavelet of order 4. The results of the *sureshrink* can be seen in Fig. 10, along with comparison against the minimum RMSE obtained for the loess smoothing.

The horizontal line on the Figure indicates the level of error for the best loess filter. It may be seen that none of the wavelets from either the S-PLUS based shrinking or those from the R *sureshrink* analysis (Table 1) are an improvement on this. It is also apparent that in general, the lower orders of wavelets perform better than those of higher orders.

Wavelets would seem to be effective in noise reduction, although in this instance inferior to loess regression. A particular concern is the slightly arbitrary choice of wavelet function, this currently being dictated by those functions being made available in the relevant R and S-PLUS libraries. However, it is worth noting that there were no outstanding winners' among the wavelet functions, with similar results in terms of RMSE being recorded for all kinds of wavelet. One observation from the *sureshrink* analysis perhaps worth re-iterating is that lower order wavelets seem to perform relatively well-suggesting a dictum of simpler is better'?

Although in this instance wavelet analysis was inferior to loess regression for smoothing/filtering the noise, this may be due to the specific mechanism chosen to generate the errors in the experiment. Although our method provided a useful insight in terms of real world' errors, further work is needed to see whether the observations made on the basis of our error

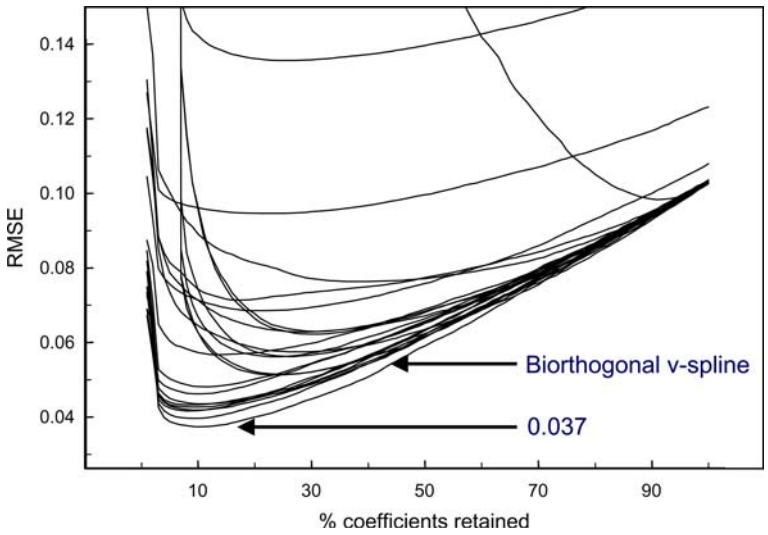

Fig. 8 Performance of S-PLUS 2D DWT wavelet shrinkage. *Each line* represents a different wavelet

modelling would be reproduced in other terrains. Alternative error distributions that may arise from other situations, and which exhibit different patterns of autocorrelation, may result in different outcomes. Thus, there is a need to investigate other terrains, and also to consider theoretical approaches to error simulation, so that results of assessing filters on error with known statistical properties can be obtained. For example, smoothing splines (see for example Wahba 1975) may be considered as an alternative to

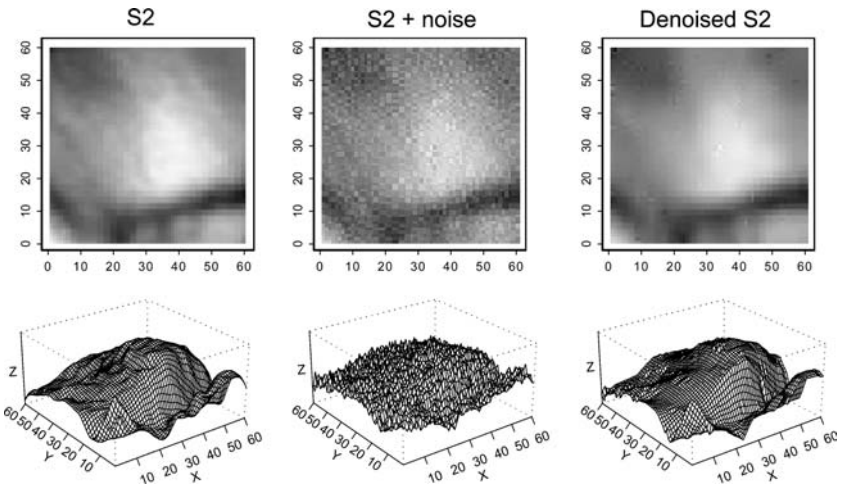

Fig. 9 Images and perspective views of S2 before/after wavelet shrinkage

Table 1 Wavelets used in the sureshrink analysis

Wavelet type	Orders used	Annotation in Fig. 10
Haar	n/a	haar
Daubechies (extremal phase)	4, 6,8,16	d4,d6,d8,d16
Daubechies (least asymmetric)	8,16,20	la8,la16,la20
Minimum bandwidth	4,8,16,24	mb4,mb8,mb16,mb24
Fejer–Korovkin	4,6,8,14,22	fk4,fk6,fk8,fk14,fk22

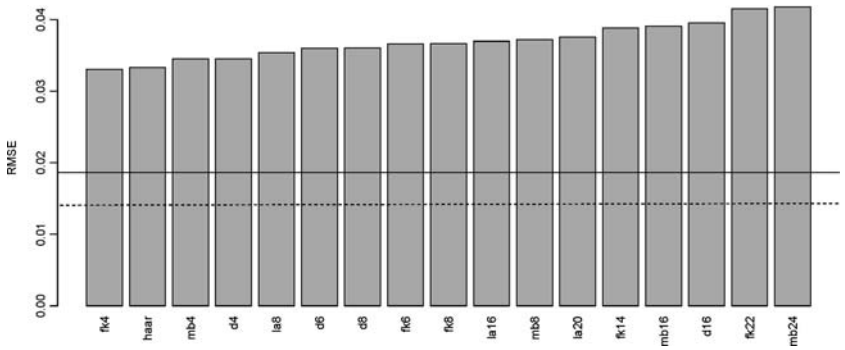

Fig. 10 Performance of the R *sureshrink* algorithm—see Table 1 for explanation of *x*-axis labels. The *horizontal lines* indicate the minimum RMSE for linear (*solid line*) and quadratic (*dashed line*) loess regressions

either wavelets or local regression smoothing. It is intended that these will be topics of future investigation.

5 Conclusions

Comparison of the effectiveness of the loess regression and wavelet methods for smoothing/filtering the sample LiDAR DSM reveals that the loess regression smoothing method produces a surface with a lower RMSE than either of the wavelet denoising methods. On the basis of this study loess regression would seem to be a preferable method for noise reduction, however, these findings undoubtedly reflect the specific characteristics study area used for the assessment, and cannot be said to any more than indicative without application of the methods to a variety of LiDAR-derived DSMs of contrasting terrain type/landcover. The degree to which this finding is a function of the particular error model and scale of feature encountered in this study also requires further research.

Acknowledgements The LiDAR dataset was kindly supplied by the National Centre for Environmental Data and Surveillance, Environment Agency, Bath. We are grateful to Andrew Large and Malcolm Newson of the University of Newcastle, and Ian Fuller of Massey University New Zealand for collaboration on an earlier stage of this research. Thanks are also extended to Professor Michael Goodchild for permission for the use of

his image in Fig. 2, the Cartography Unit at the Department of Geography University of Leicester for preparing Figs. 2 and 3, and the anonymous referees for some useful suggestions that improved the paper.

References

Abramovich F, Bailey TC, Sapatinas T (2000) Wavelet analysis and its statistical applications. The Statistician 49(1):1–29

Albani M, Klinkenberg B (2003) A spatial filter for the removal of striping artifacts in digital elevation models. Photogram Eng Remote Sens 63:755–766

Argenti F, Alparone L (2002) Speckle removal from SAR images in the undecimated wavelet domain. IEEE Trans Geosci Remote Sens 40(11):2363–2374

Atkinson PM (2001) Geographical Information Science: Geocomputation and non-stationarity. Prog Phys Geogr 25(1):111–122

Bjørke JT, Nilsen S (2003) Wavelets applied to simplification of digital terrains. Int J Geogr Inf Sci 17(7):601–621

Bruce A, Gao H-Y (1995) Applied wavelet analysis with S-PLUS. Springer, Berlin, Heidelberg, New York

Charlton ME, Large ARG, Fuller IC (2003) Application of airborne LiDAR in river environments: the River Coquet, Northumberland, UK. Earth Sur Land 28:299–306

Cleveland WS, Loader CL (1996) Smoothing by local regression: principles and methods. In: Haerdle W, Schimek MG (eds) Statistical theory and computational aspects of smoothing. Springer, Berlin Heidelberg, New York, pp 10–49

Cleveland WS, Grosse E, Shyu WM (1992) Local regression models. In: Chambers JM, Hastie TJ (eds) Statistical models in S. Chapman and Hall, New York, pp 309–376

Csillag F, Kabos S (2002) Wavelets, boundaries and the spatial analysis of landscape pattern. Ecoscience 9(2):177–190

Dai M, Peng C, Chan AK, Loguinov D (2004) Bayesian wavelet shrinkage with edge detection for SAR image despeckling. IEEE Trans Geosci Remote Sens 42(8):1642–1648

Daubechies I (1992) Ten lectures on wavelets. Society for Industrial and Applied Mathematics, Philadelphia

Davis GM, Nosratinia A (1999) Wavelet-based image coding: an overview. In: Datta BN (ed) Applied and computational control, signals, and circuits vol. 1. Birkhauser, Boston, pp 205–269

Donoho DL, Johnstone IM (1995) Adapting to unknown smoothness via wavelet shrinkage. J Am Stat Assoc 90:1200–1224

Dubayah R, Knox R, Hofton M, Blair JB, Drake J (2000) Land surface characterization using lidar remote sensing. In: Hill M, Aspinall R (eds) Spatial information for land use management. International Publishers Direct, Singapore, pp 25–38

Fukuda S, Hirosawa H (1998) Suppression of speckle in synthetic aperture radar images using wavelet. Int J Remote Sens 19(3):507–519

Gallant JC, Hutchinson MF (1997) Scale dependence in terrain analysis. Math Comput Simul 43:313–321

Graps A (1995) An introduction to wavelets. IEEE Comput Sci Eng 2(2):50–61

Hubbard BBH (1996) The world according to wavelets: the story of a mathematical technique in the making. Mass: A. Peters, Wellesley

Huising EJ, Gomes-Pereira LM (1998) Errors and accuracy estimates of laser data acquired by various laser scanning systems for opographic applications. ISPRS J Photogram Remote Sens 53:245–261

Jiang XQ, Blunt L, Stout KJ (2000) Development of a lifting wavelet representation for surface characterization. In: Proceedings of the royal society of London A 456:2283–2313

Kumar P, Foufoula-Georgiou E (1997) Wavelet analysis for geophysical applications. Rev Geophys 35(4):385–412

Lark RM, Webster R (1999) Analysis and elucidation of soil variation using wavelets. Eur J Soil Sci 50:185–206

Lark RM, Webster R (2004) Analysing soil variation in two dimensions with the discrete wavelet transform. Eur J Soil Sci 55:777–797

Lillesand TM, Kiefer RW, Chipman JW (2004) Remote sensing and image interpretation. Wiley, New York
Lòpez C (2002) An experiment on the elevation accuracy improvement of photogrammetrically derived DEM. Int J Geogr Inf Sci 16:361–375
Mallat SG (1989) A theory for multiresolution signal decomposition: the wavelet representation. IEEE Trans Pattern Anal Mach Intell 11:674:693
McArthur DE, Fuentes RW, Devarajan V (2000) Generation of hierarchical multiresolution terrain databases using wavelet filtering. Photogram Eng Remote Sens 66(3):287–295
Morehart M, Murtagh F, Starck J-L (1999) Spatial representation of economic and financial measures used in agriculture via wavelet analysis. Int J Geogr Inf Sci 13(6):557–576
Myers DE (1989) To be or not to be... stationary? That is the question. Math Geol 21:347–362
Newson MD (2005) Environmental capital: strategic and operational guide to the River Coquet Northumberland and additional experiences from the River Wharfe. J Environ Plan Manage (in press)
Press WH, Teukolsky SA, Vetterling WT, Flannery BP (1992) Numerical recipes in fortran 77: the art of scientific computing. Cambridge University Press, Cambridge
Rosenberg MS (2004) Wavelet analysis for detecting anisotropy in point patterns. J Veg Sci 15:277–284
Schmidt J, Evans IS, Brinkmann J (2003) Comparison of polynomial models for land surface curvature calculation. Int J Geogr Inf Sci 17(8):797–814
Stein C (1981) Estimation of the mean of a multivariate normal distribution. Ann Stat 9:1135–1151
Strang G (1994) Wavelets. Am Sci 82:250–255
Taswell C (2000) The what how and why of wavelet shrinkage denoising. Comput Sci Eng 2(3):12–19
Taubman DS, Marcellin MW (2001) JPEG200: image compression fundamentals, standards and practice. Kluwer, Dordrecht
Wahba G (1975) Smoothing noisy data by spline functions. Numer Math 24:383–393
Wang Z (1998) Applying two-dimensional Kalman filtering techniques to digital elevation models for terrain surface modelling. In: Fritsch D, Englich M, Sester M (eds) ISPRS commission iv symposium on GIS—between visions and applications, International Archives of Photogrammetry and Remote Sensing vol. 32/4 Stuttgart Germany pp 649–656
Wang Z, Trinder J (2002) Wavelet transform based noise removal for terrain surface modelling. The 11th Australasian remote sensing and photogrammetry association conference. Brisbane, Australia, pp 877–884
Wehr A, Lohr U (1999) Airborne laser scanning—an introduction and overview. ISPRS J Photogram Remote Sens 54:68–82
Whitcher B (2004) Software, Retrieved 12 December 2004 from http://www.cgd.ucar.edu/stats/staff/whitcher/software/
Wood JD (1996) The geomorphological characterisation of digital elevation models. Department of Geography, University of Leicester, UK
Wood JD (1998) Modelling the continuity of surface form using digital elevation models. In: Poiker T, Chrisman N (eds) Proceedings of the 8th international symposium on spatial data handling. pp 725–36
Zatelli P, Antonello A (2002) New GRASS modules for multiresolution analysis with wavelets. In: Proceedings of the open source GIS-GRASS users conference 2002, Trentino, Italy, 11–13 September 2002 pp 1–27